Journal of Physics: Condensed Matter

PAPER

Role of tetrahedrally coordinated dopants in palladium hydrides on their superconductivity and inverse isotope effect

To cite this article: S Ostanin *et al* 2019 *J. Phys.: Condens. Matter* **31** 075703

View the article online for updates and enhancements.

IOP ebooks™

Bringing you innovative digital publishing with leading voices to create your essential collection of books in STEM research.

Start exploring the collection - download the first chapter of every title for free.

This content was downloaded from IP address 192.108.69.177 on 19/07/2019 at 11:45

IOP Publishing Journal of Physics: Condensed Matter
J. Phys.: Condens. Matter **31** (2019) 075703 (6pp) https://doi.org/10.1088/1361-648X/aaf5b0

Role of tetrahedrally coordinated dopants in palladium hydrides on their superconductivity and inverse isotope effect

S Ostanin[1,2], V Borisov[1,2], D V Fedorov[2,3], E I Salamatov[4], A Ernst[2,5] and I Mertig[1,2]

[1] Institute of Physics, Martin Luther University Halle-Wittenberg, D-06099 Halle, Germany
[2] Max Planck Institute of Microstructure Physics, Weinberg 2, D-06120 Halle, Germany
[3] Physics and Materials Science Research Unit, University of Luxembourg, Luxembourg City, L-1511 Luxembourg
[4] Udmurt Federal Research Center of the Ural Branch of Russian Academy of Sciences, 34 T. Baramzinoy Str., 426067 Izhevsk, Russia
[5] Institute of Theoretical Physics, Johannes Kepler University, 4040 Linz, Austria

E-mail: vladislav.s.borisov@gmail.com

Received 1 August 2018, revised 12 November 2018
Accepted for publication 3 December 2018
Published 7 January 2019

Abstract

Absorption of hydrogen by palladium causes PdH to become superconducting below $T_c \approx 9\ K$. Due to the presence of one octapore and two tetrapores per each Pd atom, it is believed that T_c of $PdH_{x>1}$ should increase further. Here, using *ab initio* calculation we show that (i) H placed in tetrapores of PdH_x induces a wide optical gap in the phonon density of states, which significantly reduces the electron–phonon coupling, and that (ii) the energetically preferable octapores filled by H enable the 9 K superconductivity only. This scenario may close a long-standing problem of the high-T_c palladium hydrides. Moreover, simulating the pore population by H and D, within *ab initio* molecular dynamics, we are able to explain the inverse isotope effect in the framework of the Bardeen–Cooper–Schrieffer theory.

Keywords: electron–phonon interaction, superconductivity, density functional theory, inverse isotope effect

(Some figures may appear in colour only in the online journal)

1. Introduction

Amongst all conventional superconductors known to date, palladium hydrides are the most enigmatic [1]. The absorption of hydrogen by a non-superconductive Pd increases the transition temperature (T_c) of PdH_x up to 9 K [2, 3]. In the face centered cubic structure, there are one octahedrally coordinated and two tetrahedrally coordinated interstitial sites per each Pd, which will be referred below as the octapores (O) and tetrapores (T). Although the limit of absorption at ambient pressure is $x \sim 0.7$, the researchers have sporadically made their attempts [4–6] to prepare $PdH_{x>1}$, expecting that its T_c is to be significantly larger than 9 K. However, the evidences of sensationally high T_c were not reported so far.

While the H-rich palladium hydrides ($x > 1$) are still questionable, their accessible compositions display the so-called inverse (negative) isotope effect (IIE), which was found [7–9] in the 1970s, shortly after the discovery of superconductivity. The IIE, i.e. the 2 K increase of T_c, seen in PdD_x between $0.7 \leqslant x \leqslant 1$, as compared to PdH_x, formally contradicts the expectations of the Bardeen–Cooper–Schrieffer (BCS) theory. The latter successfully evaluates conventional superconductors utilizing the Eliashberg spectral function, which describes the coupling between the lattice vibrations and electrons as

 © 2019 IOP Publishing Ltd Printed in the UK

the product of the phonon density of states, $F(\omega)$, and the coupling constant to electrons. The BCS theory, within the harmonic approximation, estimates T_c as a function of ion mass: $T_c \sim 1/M^{\alpha}$, where the isotope coefficient α is close to 0.5. In palladium hydrides, however, α is negative and this phenomenon is still a subject of extensive theoretical debate.

The early models which can explain the IIE qualitatively, used the anharmonic effects [10] together with the isotope-dependent Debye–Waller factor or, alternatively, together with the spin paramagnon and Coulomb interactions [11, 12]. Then, the anharmonic effects were combined together with the thermal-energy fluctuations [13]. The effect of spin fluctuations on T_c and isotope effect was calculated [14] as well.

At present time, the parameter-free *ab initio* based theory [15, 16] can be used to study the IIE. For instance, the computational model which includes stochastic ionic vibrations has been proposed recently [17, 18] to evaluate the IIE. By treating hydrogen vibrations far beyond harmonic, Errea *et al* [17, 18] obtained $\alpha = -0.38$ that seems to solve the problem. Despite the fact that exaggerated anharmonicity triggered by quantum fluctuations can quantitatively explain the inverse isotope effect in palladium hydrides [17, 18], there is no explicit explanation why this material is so unique and why the similar exaggerated anharmonic effects were not detected in other hydrides of the transition metals. The previous theoretical studies deal with static configurations of dopants in palladium at zero temperatures. Thus, even if quantum fluctuations were included, the researchers who try to solve the problem statically fail to address a key question: why does IIE start at $x \sim 0.7$ but not before this ambient limit of absorption?

In this work, we study PdH_x and PdD_x from first principles and demonstrate that their phonon-mediated superconductivity can be quantified by taking into account the dynamics of differently coordinated positions for dopants in octapores and tetrapores. When dopants appear in tetrapores, the phonon density of states displays a gap that dramatically reduces the electron–phonon coupling (EPC) constant to the value below the threshold of T_c. Thus, we suggest that only octapores occupied by hydrogen or deuterium enable superconductivity in palladium hydrides and, moreover, that their T_c should not increase at $x > 1$ since all excessive dopants above $x = 1$ occupy tetrapores.

2. Methods

2.1. Structural optimization of the PdH_x supercells

The electronic and lattice properties of PdH_x ($1/8 \leqslant x \leqslant 1$) were computed using the minimal supecell size, namely, Pd_8H_1 for $x = 1/8$, Pd_4H_1 for $x = 1/4$ and so on, although the larger supercells of each composition, such as Pd_8H_2, were also inspected. The structural optimization was performed using the QUANTUM ESPRESSO (QE) code [28] and Vienna *Ab initio* Simulation Package (VASP) [19], within the generalized-gradient approximation [32] to the exchange-correlation potential. The electron–ion interactions were described within the VASP calculations by projector-augmented wave

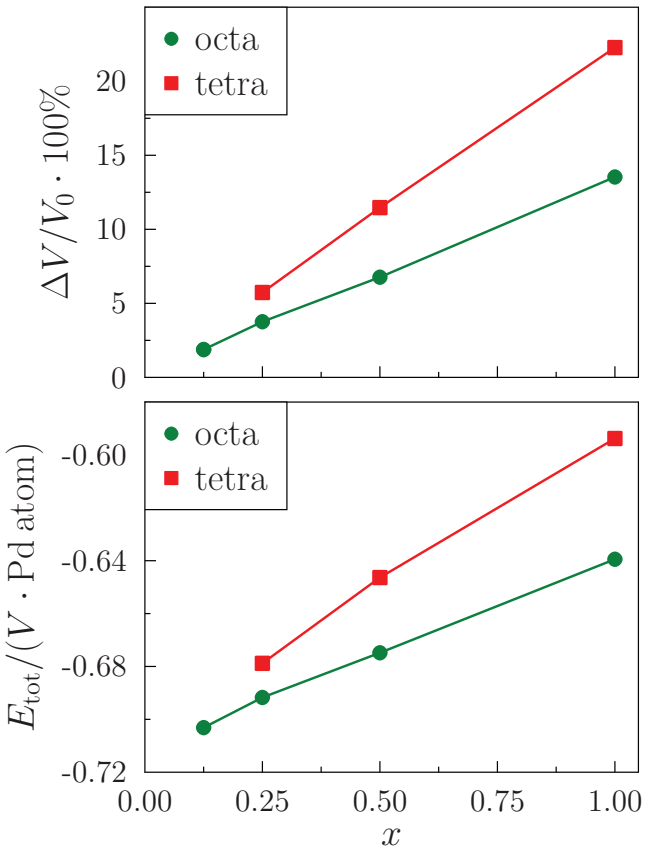

Figure 1. The total energy and equilibrium volume of PdH_x, which are plotted in the lower and upper panels, respectively, versus x for both the octahedral and tetrahedral positions of hydrogen.

pseudopotentials [33], and the electronic wave functions were represented by plane waves with a cutoff energy of 450 eV. Ionic relaxation of the PdH_x supercells was performed using the Γ-centered $6 \times 6 \times 6$ k-point Monkhorst–Pack mesh and the conjugate-gradient algorithm until the Hellmann–Feynman forces became less than 5×10^{-3} eV Å^{-1}, which yielded reliable results for the atomic positions. The structural optimization was followed by calculations of the electronic and lattice properties for each composition of PdH_x. The equilibrium volume of PdH_x calculated for $0 \leqslant x \leqslant 1$ and related energetics are plotted in figure 1. For $x = 1$, when hydrogen occupies octapores (tetrapores) the volume increase is about 13% (20%). The density of states (DOS) was obtained using the tetrahedron method on the Γ-centered $8 \times 8 \times 8$ **k**-mesh with no smearing for the electronic occupations. The detailed Fermi surfaces of Pd and PdH were calculated using the relativistic Korringa–Kohn–Rostoker method [34].

2.2. Ab initio MD simulations

To simulate the pore population by dopants we used the 64-atom Pd supercell, the tetrapores and octapores of which accomodate between 46 and 64 hydrogens or, alternatively, D species that covers the PdH_x compositions $0.7 \leqslant x \leqslant 1$. For each supercell the *ab initio* molecular dynamics simulations were performed using the code VASP [19]. The electron

orbitals were represented using plane-waves, with a cut-off energy of 400 eV, while the electron–ion interactions were described by the PAW pseudopotentials [33]. The conclusions of our simulations are completely unaffected by the approximation to the exchange-correlation potential. All dopants were allowed to move while the time step was 1 fs. To obtain adequate statistics for thermodynamic equilibrium, we run a set of simulations for a time of 10 ps, keeping the different temperatures which were varied between 10 K and 200 K. Since the simulations were started from artificially chosen and different initial positions of H(D), we excluded the first 30 fs outputs from the statistics.

2.3. Phonon frequencies

The phonon frequencies were calculated for each accurately optimized structure within the QE code [28]. To avoid the phonon mode softening, which can happen already at $\mathbf{q} = (0,\ 0,\ 0)$ before the structural optimization and which indicates the lattice instability of the system at $T = 0$ K, we performed further relaxation of atomic positions and the cell shape. After relaxation, the structures can show some minor (below 0.5%) rhombohedral distortions. For the decomposition of the wavefunctions and charge density, we used the plane-wave cutoff energies of 40 Ry and 280 Ry, respectively. All electronic structure calculations were performed within the generalized-gradient approximation [32], using the Γ-centered $(8 \times 8 \times 8)$ k-point mesh while denser $(16 \times 16 \times 16)$ k-mesh was utilized to compute the electron–phonon coupling. Regarding the phonon frequencies, $\omega_i(\mathbf{q})$, the dynamical matrices were calculated for each $\mathbf{q}$ of the Brillouin zone $(4 \times 4 \times 4)$ mesh and, then, the resulting real-space atomic force constants were obtained using the Fourier transformation. The scheme [16] provides the phonon frequencies of sufficiently good accuracy, as compared to that of directly calculated from the much more computationally demanding finite-displacement supercell method. In the case of fcc-Pd, for instance, the phonon dispersion curves are in a good agreement with the experimental data and previously reported *ab initio* results [20]. The phonon density of states was calculated using the tetrahedron method.

2.4. Electron–phonon coupling

Using the phonon dispersion curves over the Brillouin zone we calculated the Eliashberg spectral function (ESF), $\alpha^2F(\omega)$, and also the electron–phonon coupling (EPC) parameter λ [15, 16]. Then the superconducting temperature, T_c, can be estimated simply from the McMillan formula:

$$T_c = \frac{\langle\omega\rangle}{1.2} \exp\left\{-\frac{1+\lambda}{0.96\lambda - \mu^*(1+\lambda\,\langle\omega\rangle/\omega_{\max})}\right\}, \quad (1)$$

where $\langle\omega\rangle$ is the weighted phonon frequency defined as follows:

$$\langle\omega\rangle^2 = \frac{\int_0^{\omega_{\max}} \omega\alpha^2F(\omega)\mathrm{d}\omega}{\int_0^{\omega_{\max}} \omega^{-1}\,\alpha^2F(\omega)\mathrm{d}\omega} \quad (2)$$

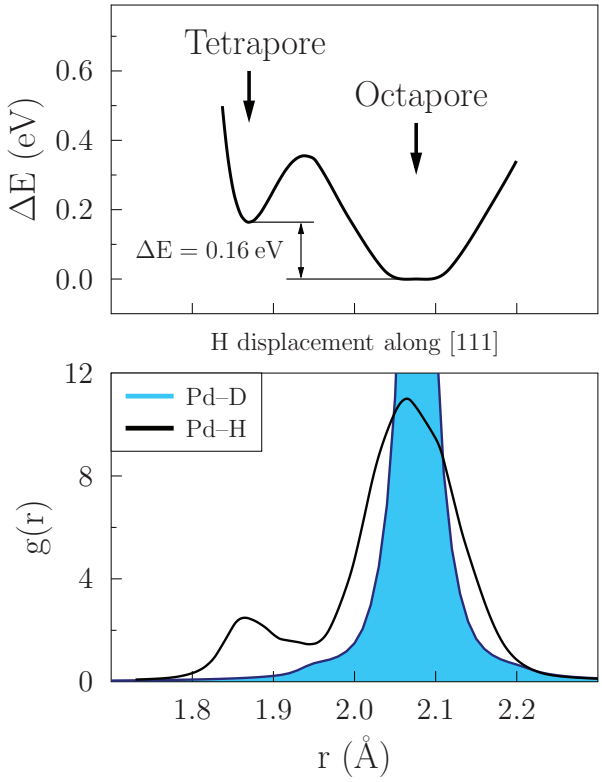

Figure 2. The energy profile of PdH, which is plotted in the top panel, was calculated for an H dopant displaced in fcc-Pd along [1 1 1] through one tetrapore and octapore. In the lower panel, the radial distribution functions plotted versus r, the distance between Pd and H(D) species, are shown for PdH (black line) and PdD (shaded area).

and μ^* is the Coulomb pseudopotential. Frequently, μ^* is treated empirically to fit the T_c estimate to the known experimental value. Here, for palladium hydrides we used simply the adjusted value of $\mu^* = 0.18$ which is slightly larger than the standard value of 0.13 for metals. For comparison, Papaconstantopoulos *et al* [21] used relatively small adjusted value of 0.085 that is, mostly, because of utilization of neutron-scattering data.

3. Results

3.1. Ab initio molecular dynamics simulations

The H(D) dopants show large diffusion coefficient in Pd and, therefore, they can migrate in the host lattice due to quantum tunneling [1]. Prior to the modelling of the pore population in PdH_x and PdD_x, we optimized the crystal structure of PdH_x, using the supercell approach and the VASP code [19]. For hydrogen, its position in octapore is energetically favourable by 0.16 eV with respect to the T-pore, as shown in the top panel of figure 2. The energy barrier was simulated for the Pd_4H_1 supercell. The two minima of the energy profile along [1 1 1] are separated by the barrier of about 0.35 eV. This result is consistent with previously reported *ab initio* study [22] of PdH_x, while the quantitative deviations can appear there since the energy profile depends significantly on the obtained equilibrium volume of the PdH_x supercell and its composition. Ke

and Kramers [23] reported that when the zero point energy is included the O-pore position for hydrogen in PdH_x is 81 meV more stable than tetrapore. Thus, the zero point motions significantly increase the O-pore stability [23]. Further improvement of the pore energetics can be achieved using the free energy contributions, such as the electronic entropy and vibrational entropy terms [24]. In this work, however, we calculated simply the total energies aiming to illustrate that the barrier shape in figure 2 qualitatively agrees with that reported by Ke *et al* [23]. Besides, the potential profile was calculated here keeping the equilibrium volume fixed for the case of occupied octapore. However, the equilibrium volumes for hydrogen in tetrapore and octapore are different that is shown clearly in figure 1. This volume difference therefore may be responsible for the more unfavorable dopant position in tetrapore that was demonstrated by Ke and Kramers [23].

The controversy over the occupation by deuterium of tetrahedral interstices in palladium was studied experimentally [25]. The model of tetrahedral occupancy was necessary there to fit the experimental diffraction profiles. At the D:Pd atomic ratio of 0.6, about one-third of all D were in tetrahedral sites. With increasing deuterium concentration, the tetrahedral fraction decreases dramatically. This experimental result should remove a conceptual concern expressed by Ke and Kramers [23] regarding tetrahedral occupancy in palladium hydrides.

Based on the calculated energy profile of the material, which is shown in figure 2, one can suppose that below the absorption limit hydrogen and deuterium firstly occupy energetically favorable octapores. To reveal the difference between these two light species, we performed *ab initio* molecular dynamics (MD) simulations. The use of the 64-atom Pd supercell, the pores of which can accommodate between 46 and 64 dopants allows to simulate PdH_x for $0.7 \leqslant x \leqslant 1$. The larger host supercells were also examined. We calculated the partial radial distribution function (RDF), $g_{\alpha\beta}(r)$, defined so that sitting on an $\alpha = \mathrm{Pd}$ atom the probability of finding the light β-atom in the spherical shell $(r, r + \mathrm{d}r)$ is $4\pi r^2 n_\beta g_{\alpha\beta}(r)\mathrm{d}r$, where n_β is the number density of the β species.

In figure 2 we plot the two RDFs calculated for Pd-H and Pd-D separations, which were simulated over the long time interval at 10 K. The temperature variation below 200 K gives the minor effect on RDF. Each RDF in figure 2 shows its main peak, which corresponds to the O-pore position at the distance of $a/2$ to Pd, where a is the lattice parameter. In the case of H, nevertheless, the shorter Pd-H separation of $a\sqrt{3}/4$, which is related to the T-pore, seems quite possible. From the shape of RDF we conclude that deuteriums tend to occupy all available octapores whereas hydrogens are distributed between the O- and T-pores as 10:1. In practice, this ratio can decrease when the H pressure is used to exceed the absorption limit of $x \sim 0.7$. Importantly, for $0.7 \leqslant x \leqslant 1$ the probability to find H in tetrapores is larger compared to D. A crucial consequence of this disproportion on T_c is discussed below. It should be noted that although the RDF simulated here are anharmonic the subsequent and presented below calculations are confined to the harmonic approximation.

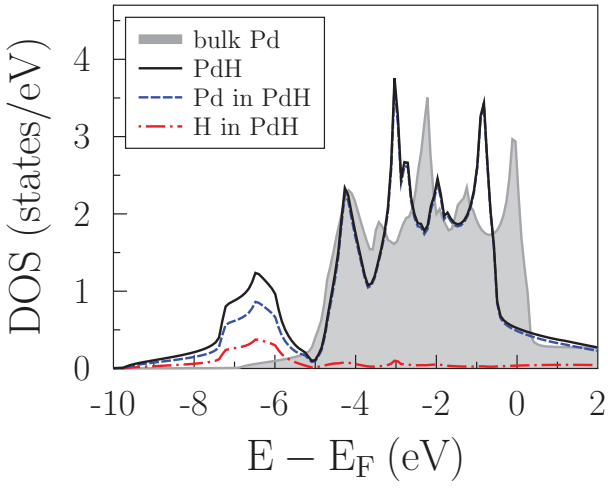

Figure 3. The total DOS calculated for Pd and PdH^O with H in octapores. For PdH^O the site-projected DOS are shown for comparison.

3.2. Electronic structure and Fermi surface

The electronic and lattice properties of PdH_x were computed for $x = 1/8$, $x = 1/4$, $x = 1/2$ and $x = 1$. Because the details of electronic structure are not distinctive between PdH and PdD, we discuss the case of PdH_x. With increasing x, the equilibrium volume gradually increases so that when the H content in octapores reaches 100 at.% the volume increases by 13% compared to that of pure Pd. The density of states (DOS) of PdH^O, which corresponds to the case when H occupy all octapores, is plotted in figure 3. One can see that the *s*-states of H are localized about 6 eV below the Fermi level (E_F) and, therefore, these states should not contribute significantly to the DOS at E_F. However, due to the lattice expansion caused by hydrogen, the *d*-band of PdH^O becomes narrower, as compared to bulk Pd. Simultaneously, since PdH^O is the electron-doped Pd, its *d*-band top is now 0.25 eV below E_F. As a result, the Pd $s-p$ states appear at E_F that transforms the FS of PdH^O, making it similar to the FS of Ag. As shown in figure 4, the FS of PdH^O has a single sheet having open necks along [1 1 1] in the Brillouin zone, whereas the FS of Pd displays three sheets, which are formed by the Pd *d*-states. The difference in the FS topology between Pd and PdH and the corresponding change from the *d* to $s-p$ character is decisive in the context of superconductivity.

3.3. Phonons and electron–phonon coupling

Recently, two groups of authors calculated the phonon frequencies of PdH^O, using the different *ab initio* based approaches, beyond the harmonic approximation [26, 27]. For PdH^T, the phonon dispersions were not reported so far. In this work, the phonon frequencies and ESF of PdH_x^O and PdH_x^T were calculated using the pseudopotential plane-wave method as implemented in the QE package [28]. Afterwards, by integrating the ESF over phonon frequencies ω, the electron–phonon

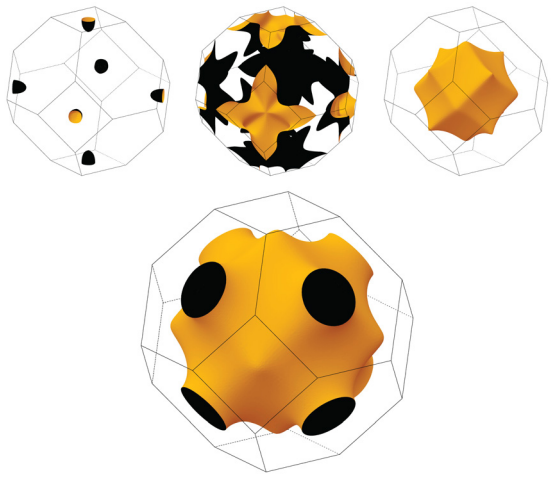

Figure 4. The three-sheeted Fermi surface (FS) of Pd shown in three upper panels and FS of PdH^O shown below.

coupling constant, λ, was obtained that provides the estimate of T_c.

When each kind of dopants relax, for instance, in tetrapores the phonon density of states, $F(\omega)$, differs dramatically from that of octapores, as shown in figure 5. Surprisingly, for tetrahedrally coordinated hydrogen in PdH^T we found rather significant gap of 19 THz in $F(\omega)$, which exists throughout the whole interval of simulated concentrations $\frac{1}{8} \leqslant x \leqslant 1$ and which increases with increasing x. The issue of the phonon gap has been discussed recently in the context of the thermal and thermoelectric properties [29]. Usually, the low-frequency gap is in the focus of such studies. In our case, however, dealing with the high-frequency phonon gap, we are focusing on its role on the ESF and superconductivity.

4. Discussion

For the binary systems, the gap in $F(\omega)$ may appear as the result of the large mass disproportion between two species. In some compounds, the gap breaks $F(\omega)$ into the acoustic and optical regions. The vibrational frequency of light dopant $\omega_l^2 = \gamma/M_l$ can lie as well as below and above the topmost mode ($\omega_{\max}$) of the host lattice. When ω_l is significantly larger than $\omega_{\max}$, the high-frequency phonon branches appear above $\omega_{\max}$. For the Pd lattice we obtained $\nu_{\max}^{Pd} \approx 6.5$ THz, whereas weakly dispersed ω_l^T calculated by QE for hydrogen in the T-pore position varies between 25 THz and 32 THz. For the heavier dopant, D, placed in the T pore, its topmost phonon DOS is localized between 18 THz and 23 THz as shown in figure 5. It should be noted that the supercell approach, which is used here to model PdH_x, means that dopants form their regular sublattice. As shown in figure 5, the model yields the localized optical phonon branches, associated directly with H/D in tetrapores. The dispersionless vibrational frequencies of interstitial dopants, which can be calculated, within the harmonic approximation, using few small displacements of dopant from its equilibrium position, were reported previously [30]. This approach tends to overestimate the H/D

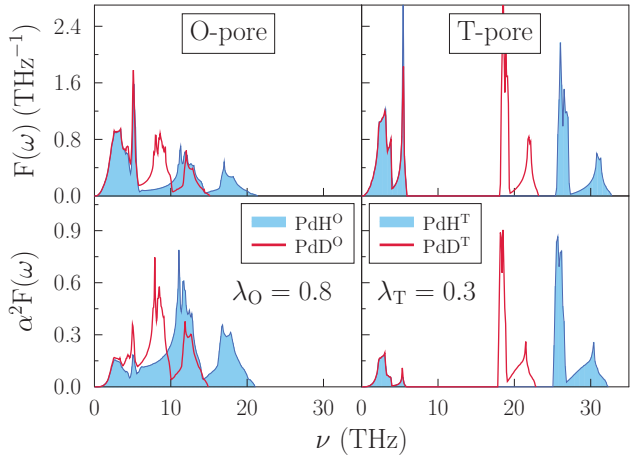

Figure 5. The phonon DOS (upper panels) and ESF (lower panels) of palladium hydrides calculated for $x = 1$ and for each dopant placed either in the octapore or, alternatively, in tetrapore. The calculated coupling parameter λ is shown for PdH only.

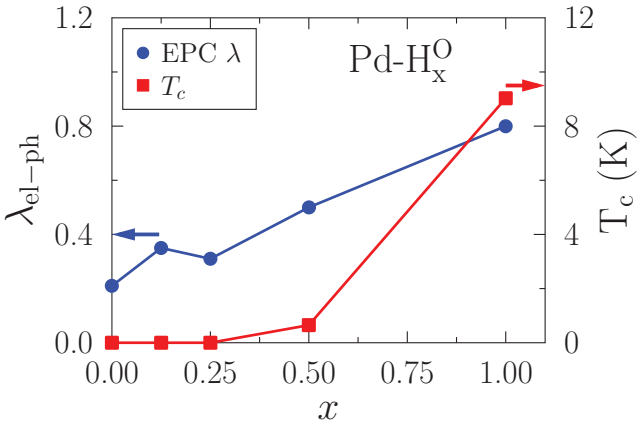

Figure 6. The electron–phonon coupling parameter and estimated T_c of PdH_x^O, calculated for H in octapores and plotted as a function of x.

vibrations in palladium hydrides, compared to the phonon DOS calculated by QE.

Regarding randomly distributed impurities and their vibrational modes, the corresponding model results were reported by Dederichs and Zeller [31]. These authors, using the Green function method for the imperfect lattice, showed how the localized mode: $\omega_l > \omega_{\max}$ appears and found the conditions for its lower and upper bounds, within the Einstein approximation. Thus, the analytical derivation confirms our *ab initio* based calculation. Since all local modes $\omega_l > \omega_{\max}$ are characterized by the effective force constant and effective mass, the comparison between ω_l^T and ω_l^O can be easily obtained. For octapore, its potential well, seen in figure 2, is wider. It means that $\gamma_{\text{eff}}^O < \gamma_{\text{eff}}^T$ and, hence, $\omega_l^O < \omega_l^T$.

As a result of the phonon gap formed in PdH^T, its ESF is also gapped. Thus, the coupling parameter to electrons becomes relatively small there: $\lambda^T = 0.3$. Although the phonon gap of PdD^T is reduced by almost 5 THz, compared to that of PdH^T, its EPC remains relatively low, below the T_c threshold. Regarding the octahedrally coordinated dopants,

we found that below $x \leqslant \frac{1}{4}$ the optical phonon modes are marginally split by 1.3 THz ($x = 1/8$) and 2 THz ($x = 1/4$). However, when x approaches 50 at.% the gap in $F(\omega)$ completely disappears that yields robustly strong EPC. For PdH^{O}, as shown in figure 5, we obtained $\lambda^{O} = 0.8$, which is strong enough to enable superconductivity.

Using the McMillan formula we estimated the critical temperature magnitude for the two coordinations of H and for each x modeled. In figure 6, this T_c is plotted as a function of x. For $PdH^{O}_{x=1}$, our calculation of T_c is in a very good agreement with the experiments. For $x \leqslant 1$ the $T_c > 0$ values start from $x = 0.5$ and for dopants relaxing in the O-pores only. If tetrapores are filled by H or D then the phonon gap notably separates the dopant-associated optical modes that, therefore, weakens λ. The features of $F(\omega)$ and ESF shown in figure 5 for PdH^{T}_{x} illustrate that. These findings are important for the clarification of IIE.

5. Summary

From our simulations it can be concluded that the Pd octapores are more favourable energetically for H(D) than tetrapores. On the other hand, D as heavier species tend to occupy octapores at $x \leqslant 1$ whereas H can appear in tetrapores even if there are empty O-pores. Meanwhile, when dopants occupy tetrapores, their phonons display the gap, which dramatically diminishes the EPC figure of merit to the values below the threshold needed for T_c. Thus, we suggest that only octapores filled with H(D) support superconductivity in the material. Regarding the IIE, we suggest also that for the given concentration $0.7 \leqslant x \leqslant 1$ the T_c of PdH_x may become smaller, as compared to PdD_x. This is because of lighter H, since their portion of about several percent can sit in the 'EPC-suppressing' T-pores. Unfortunately, we cannot quantify here the 2 K IIE because the temperature used in MD simulations is an uncalibrated model parameter. Finally, our findings allow to conclude that T_c of palladium hydrides should not increase for $x > 1$ since all extra dopants above $x = 1$ relax in tetrapores and environmentally do not contribute to superconductivity. We believe that this work can provoke further studies of palladium hydrides using more sophisticated dynamical models.

Acknowledgments

This work is supported by the DFG within the Collaborative Research Center *Sonderforschungsbereich* SFB 762. EIS thanks the Russian Foundation for Basic Research (project 16-07-00529), the Ural Branch of RAS (grant 18-2-2-12) and the program AAAA-A16-116021010082-8.

ORCID iDs

V Borisov https://orcid.org/0000-0001-7409-2196

References

[1] Fukai Y 2005 *The Metal-Hydrogen System* (Berlin: Springer) (https://doi.org/10.1007/3-540-28883-X)
[2] Harper J M E, Hammond R and Geballe T H 1973 *Bull. Am. Phys. Soc.* **18** 326
[3] Harper J M E 1974 *Phys. Lett.* A **47** 69
[4] Semenenko K N, Ganich E A and Yakovleva N A 2000 *Dokl. Chem.* **375** 247
[5] Tripodi P, Di Gioacchino D and Vinko J D 2004 *Braz. J. Phys.* **34** 1177
[6] Harada S, Donuma T, Araki H, Kakuta T, Nakatsuji R, Mueller R M and Kubota M 2011 *J. Low Temp. Phys.* **162** 724
[7] Buckel W and Stritzker B 1973 *Phys. Lett.* A **43** 403
[8] Schirber J E and Northrup C J 1974 *Phys. Rev.* B **10** 3818
[9] Yossouff M, Rao B K and Jena P 1995 *Solid State Commun.* **94** 549
[10] Karakozov A E and Maksimov E G 1978 *Sov. Phys.—JETP* **74** 681
[11] Zhernov A P and Drekhsler S L 1985 *Fiz. Nizk. Temp.* **11** 899
[12] Crespi V H and Cohen M L 1992 *Solid State Commun.* **83** 427
[13] Salamatov E I 1998 *Solid State Commun.* **106** 269
[14] Dolgov O V, Mazin I I, Golubov A A, Savrasov S Y and Maksimov E G 2005 *Phys. Rev. Lett.* **95** 257003
[15] Savrasov S Y 1996 *Phys. Rev.* B **54** 16470
[16] Baroni S, de Gironcoli S, Dal Corso A and Giannozzi P 2001 *Rev. Mod. Phys.* **73** 515
[17] Errea I, Calandra M and Mauri F 2013 *Phys. Rev. Lett.* **111** 177002
[18] Errea I, Calandra M and Mauri F 2014 *Phys. Rev.* B **89** 064302
[19] Kresse G and Furthmüller J 1996 *Phys. Rev.* B **54** 11169
[20] Savrasov S Y and Savrasov D Y 1996 *Phys. Rev.* B **54** 16487
[21] Papaconstantopoulos D A, Klein B M, Economou E N and Boyer L L 1978 *Phys. Rev.* B **17** 141
[22] Koroteev Y M, Gimranova O V and Chernov I P 2011 *Phys. Solid State* **53** 896
[23] Ke X and Kramers G J 2002 *Phys. Rev.* B **66** 184304
[24] Ostanin S A and Trubitsin V Y 1997 *J. Phys.: Condens. Matter* **9** L491
[25] McLennan K G, Gray E M and Dobson J F 2008 *Phys. Rev.* B **78** 014104
[26] Belov M P, Syzdykova A B, Vekilov Y K and Abrikosov I A 2015 *Phys. Solid State* **57** 260
[27] Paulatto L, Errea I, Calandra M and Mauri F 2015 *Phys. Rev.* B **91** 054304
[28] Giannozzi P *et al* 2009 *J. Phys.: Condens. Matter* **21** 395502
[29] Maldovan M 2013 *Nature* **503** 209
[30] Elsässer C, Ho K M, Chan C T and Fähnle M 1992 *J. Phys.: Condens. Matter* **4** 5207
[31] Dederichs P H and Zeller R 1976 *Phys. Rev.* B **14** 2314
[32] Perdew J P, Burke K and Ernzerhof M 1996 *Phys. Rev. Lett.* **77** 3865
[33] Blochl P E 1994 *Phys. Rev.* B **50** 17953
[34] Gradhand M, Czerner M, Fedorov D V, Zahn P, Yavorsky B Y, Szunyogh L and Mertig I 2009 *Phys. Rev.* B **80** 224413